Research article

Andrey Sushko*, Kristiaan De Greve, Madeleine Phillips, Bernhard Urbaszek, Andrew Y. Joe, Kenji Watanabe, Takashi Taniguchi, Alexander L. Efros, C. Stephen Hellberg, Hongkun Park, Philip Kim and Mikhail D. Lukin

# Asymmetric photoelectric effect: Auger-assisted hot hole photocurrents in transition metal dichalcogenides

**Abstract:** Transition metal dichalcogenide (TMD) semiconductor heterostructures are actively explored as a new platform for quantum optoelectronic systems. Most state of the art devices make use of insulating hexagonal boron nitride (hBN) that acts as a wide-bandgap dielectric encapsulating layer that also provides an atomically smooth and clean interface that is paramount for proper device operation. We report the observation of large, through-hBN photocurrents that are generated upon optical excitation of hBN encapsulated $MoSe_2$ and $WSe_2$ monolayer devices. We attribute these effects to Auger recombination in the TMDs, in combination with an asymmetric band offset between the TMD and the hBN. We present experimental investigation of these effects and compare our observations with detailed, ab-initio modeling. Our observations have important implications for the design of optoelectronic devices based on encapsulated TMD devices. In systems where precise charge-state control is desired, the out-of-plane current path presents both a challenge and an opportunity for optical doping control. Since the current directly depends on Auger recombination, it can act as a local, direct probe of both the efficiency of the Auger process as well as its dependence on the local density of states in integrated devices.

**Keywords:** Auger excitation; 2D materials; optoelectronics; transition metal dichalcogenides.

**\*Corresponding author: Andrey Sushko**, Department of Physics, Harvard University, Cambridge, Massachusetts 02138, USA, E-mail: asushko@g.harvard.edu. https://orcid.org/0000-0002-2756-9753

**Kristiaan De Greve,** Department of Physics, Harvard University, Cambridge, Massachusetts 02138, USA; and Department of Chemistry and Chemical Biology, Harvard University, Cambridge, Massachusetts 02138, USA; and Currently at Imec, Kapeldreef 75, Leuven, Belgium, E-mail: kristiaan.degreve@gmail.com

**Madeleine Phillips, Alexander L. Efros and C. Stephen Hellberg,** Naval Research Laboratory (NRL), Washington, DC 20375, USA, E-mail: madeleine.phillips.ctr@nrl.navy.mil (M. Phillips), sasha.efros@nrl.navy.mil (A.L. Efros), steve.hellberg@nrl.navy.mil (C.S. Hellberg)

**Bernhard Urbaszek,** Université de Toulouse, INSA-CNRS-UPS, LPCNO, 135 Avenue Rangueil, 31077 Toulouse, France, E-mail: urbaszek@insa-toulouse.fr

**Andrew Y. Joe, Philip Kim and Mikhail D. Lukin,** Department of Physics, Harvard University, Cambridge, Massachusetts 02138, USA, E-mail: andrewjoe@g.harvard.edu (A.Y. Joe), pkim@physics.harvard.edu (P. Kim), lukin@physics.harvard.edu (M.D. Lukin)

**Kenji Watanabe,** Research Center for Functional Materials, National Institute for Materials Science, 1-1 Namiki, Tsukuba, 305-0044, Japan, E-mail: watanabe.kenji.aml@nims.go.jp. https://orcid.org/0000-0003-3701-8119

**Takashi Taniguchi,** International Center for Materials Nanoarchitectonics, National Institute for Materials Science, 1-1 Namiki, Tsukuba, 305-0044, Japan, E-mail: TANIGUCHI.Takashi@nims.go.jp

**Hongkun Park,** Department of Physics, Harvard University, Cambridge, Massachusetts 02138, USA; and Department of Chemistry and Chemical Biology, Harvard University, Cambridge, Massachusetts 02138, USA, E-mail: Hongkun_Park@harvard.edu

encapsulating layer that also provides an atomically smooth and clean interface that is paramount for proper device operation. We report the observation of large, through-hBN photocurrents that are generated upon optical excitation of hBN encapsulated $MoSe_2$ and $WSe_2$ monolayer devices. We attribute these effects to Auger recombination in the TMDs, in combination with an asymmetric band offset between the TMD and the hBN. We present experimental investigation of these effects and compare our observations with detailed, ab-initio modeling. Our observations have important implications for the design of optoelectronic devices based on encapsulated TMD devices. In systems where precise charge-state control is desired, the out-of-plane current path presents both a challenge and an opportunity for optical doping control. Since the current directly depends on Auger recombination, it can act as a local, direct probe of both the efficiency of the Auger process as well as its dependence on the local density of states in integrated devices.

## 1 Introduction

Transition metal dichalcogenides (TMDs) [1] have recently attracted significant interest for their optoelectronic properties [2], which are dominated by strongly bound excitons. As van der Waals (vdW) 2D materials, TMDs can be incorporated into complex, high cleanliness vdW heterostructures tailored to a myriad of possible applications [3]. In particular, such systems can be used to isolate and manipulate electronic and excitonic excitations which allow the creation of engineered, controlled quantum systems [4, 5]. In general, such heterostructures rely on hexagonal boron-nitride (hBN) [6] as an atomically clean dielectric encapsulation layer to separate the active materials from each other, surrounding electrostatic gates,

and the environment [7]. Typically, these hBN layers are treated as an inert buffer whose wide 6 eV bandgap [8] allows it to serve as both a physical and electronic barrier between different parts of the heterostructure device. Deviations from this simplified picture are mostly considered in the context of trapped charge defects or dielectric breakdown.

In this article, we describe an experimental observation of a novel optoelectronic effect that challenges this simple physical picture of perfectly insulating hBN encapsulation. Specifically, we report the robust observation of a reversible, photoinduced current that appears across the thick, dielectric hBN layer. The current is observed in dozens of devices with varying geometries and hBN thicknesses, consistent with other recent reports [9, 10]. We report on a systematic doping, wavelength, electric field and thickness dependent study of this effect in two different TMD materials, which allows us to unambiguously point to Auger recombination as the central mechanism involved. Our evidence is multifold. Firstly, we observe photocurrents over a wide range of hBN thicknesses (3–90 nm in our devices) and, secondly, when deconvolved from optical doping (Supplementary Figures 4–6), it is spatially uniform throughout all devices – as verified via spatially scanning the excitation beam and by verification using split gate devices. Such uniformity and thickness independence make alternative explanations such as dielectric breakdown or tunneling via in-gap defect states in the hBN unlikely.

On the other hand, our systematic doping-, field- and wavelength dependence studies, corroborated by theoretical modeling of relevant barrier heights in the two material systems, allow us to extract a Fowler–Nordheim tunneling picture that is activated by an Auger process involving holes and excitons, which differs from previous pictures [9, 11] yet has some similarities with hot-carrier effects as previously reported in graphene-hBN heterostructures [12–14]. Crucially, this picture explains the substantial differences in photocurrent efficiency between the two materials directly from computed band alignments, without postulating significant material-dependent variation in the efficiency of Auger excitation. This process adds an important element to the physics of two-dimensional TMD devices by introducing an optically controlled transport path outside the material. Potentially, it can be leveraged to locally sink unipolar currents from an optically defined "contact" that can be arbitrarily swept over a device structure. In addition, we show that the variation in current generation efficiency can provide insight into the dynamics, transitions, and relaxation pathways of states within the TMD.

# 2 Photocurrents in encapsulated TMDs

Figure 1a shows the schematic of a typical device structure, consisting in this case of a $MoSe_2$ monolayer encapsulated in hBN over a metal gate electrode. Upon off-resonant optical excitation at 660 nm, a substantial current is measured at the bottom gate, sourced from the $MoSe_2$ via its electrical contact. This photocurrent is substantial in magnitude – up to 6 nA for an excitation power of 15 μW – and appears only in the hole doped regime, as inferred from photoluminescence (PL) emission (Figure 1b).

We first investigate the effect in detail using a dual-gated device structure in which the TMD is grounded through a side contact and the field to the top and bottom gates can be independently varied (Figure 2a). The goal of such a structure is to be able to decouple the *doping* conditions from the *electric field*, and deduce the dependence of the effect on either of them independently. Figure 2b outlines the general band alignment of the TMD/hBN/gate electrode system along with the direction of the observed current. Plotting external quantum efficiency
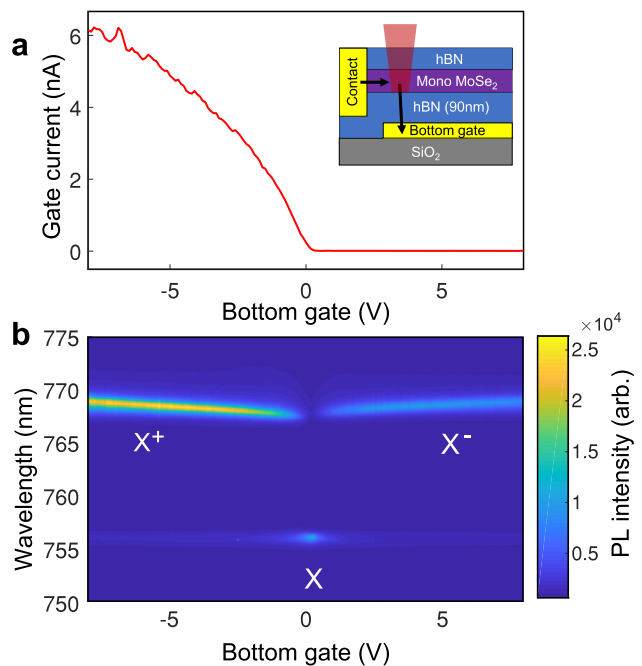


**Figure 1:** Consistent cross-hexagonal boron nitride (hBN) photocurrent.
a) Gate-voltage dependence of through-hBN photocurrent for the inset device structure (device A) under 15 μW, 660 nm optical excitation. This behavior is spatially uniform and is reproduced in a series of devices of varying hBN thickness. b) Photoluminescent emission from the same device showing presence of photocurrent in the hole doped regime.

(EQE) curves as a function of bottom gate for a $MoSe_2$ device with no top gate (Figure 2c), we first observe linear optical power dependence across three orders of magnitude, consistent with a single-photon excitation process. Here, EQE is given as the number of carriers injected into the gate per photon incident on the device structure. EQE is notably lower for the dual gate $MoSe_2$ device (Figure 2d) due to absorption of incoming photons in the metal top gate. Figure 2d, e shows the top gate current as a function of both gates for $MoSe_2$ and $WSe_2$, respectively. Cuts along the labeled lines are presented and analyzed in Figure 4. By fixing the potential difference between the TMD and the gate into which current flow is being measured, while varying the potential at the other, we can examine the doping dependence of the photocurrent process at fixed field. At a field of 0.15 V/nm (lines (1) in Figure 2d, e), both $MoSe_2$ and $WSe_2$ exhibit rapid onset of current upon hole doping, and subsequent saturation with increasing

carrier density. Similarly, by incrementing the potential on one gate, in opposition to the other, by a ratio proportional to their relative capacitance, one can maintain constant doping of the sample while varying the field (lines (2) in Figure 2d, e), thereby yielding the pure field dependence, independent of doping effects. While the doping dependences of $MoSe_2$ and $WSe_2$ appear very similar, the two materials exhibit a qualitative difference in electric field dependence, with the $MoSe_2$ current switching on rapidly at negative field while the $WSe_2$ current remains negligible until reaching a field of around 0.1 V/nm. Furthermore, even at high field, the EQE of the photocurrent in $WSe_2$ is an order of magnitude lower than what is observed in $MoSe_2$, a distinction which persists under resonant excitation (see Supplementary Figure 11). The decrease in top gate photocurrent at decreasing bottom gate voltage is attributed to competition between the two gates (see Supplementary Figure 3).
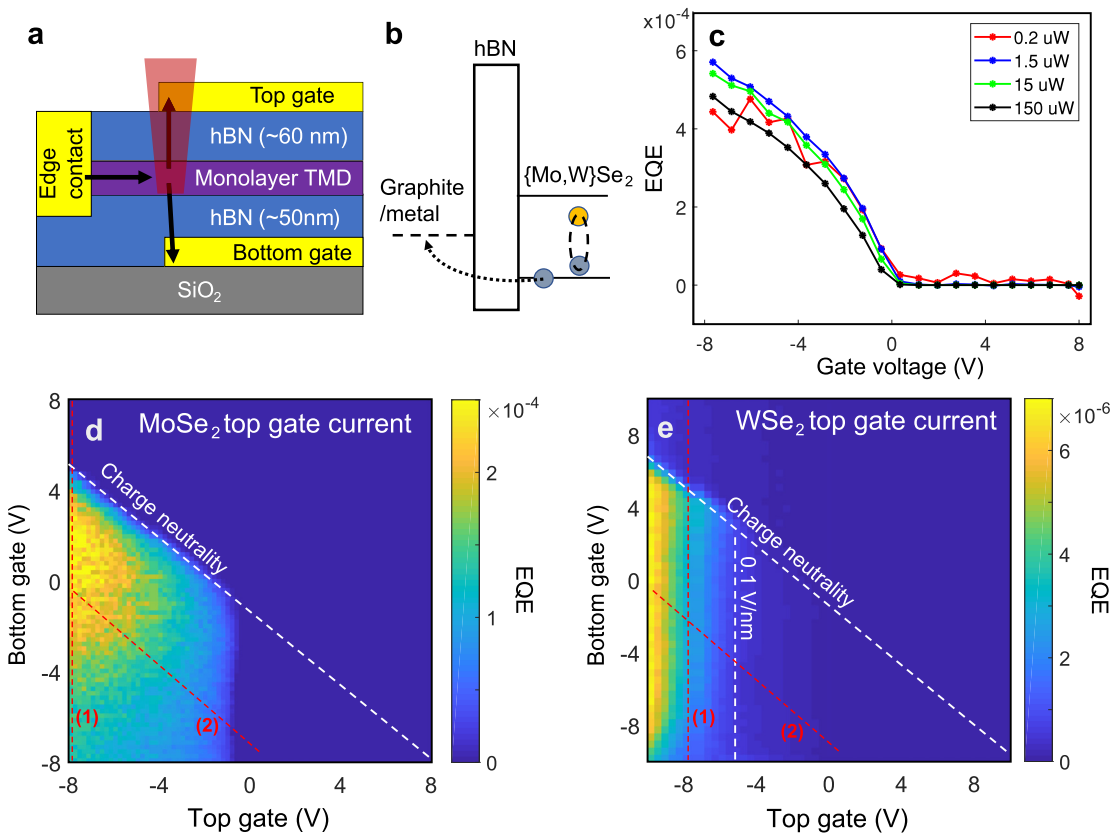


**Figure 2:** Power, field, and doping dependence in $MoSe_2$ and $WSe_2$.
a) Schematic of the dual-gated, hexagonal boron nitride (hBN) encapsulated transition metal dichalcogenide (TMD) structure designed to enable independent control of doping and electric field between the TMD and metal gates (device B). b) Band structure schematic for half of the device in (a) illustrating the hole-side photocurrent into one of the top/bottom electrodes when the TMD is hole-doped and electric field oriented toward the electrode. c) Quantum efficiency curves for a single-gated configuration (device A) show linear dependence on optical power. Here, external quantum efficiency (EQE) is the ratio of carriers through the hBN to photons incident on the heterostructure. Dependence of total current on gate conditions for $MoSe_2$ (d) and $WSe_2$ (e) shows qualitatively distinct characteristics. While both systems require hole doping, $WSe_2$ also exhibits minimal current below a field of 0.1 V/nm and much lower overall quantum efficiency relative to $MoSe_2$.

Figure 3a shows a spatial map of the photocurrent generated by scanning a diffraction limited excitation spot (see Figure 3b for the sample geometry). A graphite back gate extends under part of a MoSe$_2$ flake, vertically separated from the graphite by 3 nm hBN. This geometry produces a lateral potential step when the gate potential is adjusted relative to the TMD, as schematically shown in Figure 3c. Tuning to the hole side results in enhanced photocurrent generation along the edges of the gate. We attribute this effect to details of the hole-doping mechanism for MoSe$_2$. While the Cr/Au edge contacts are transparent to electrons, they are inefficient at injecting holes into the monolayer. The presence of an in-plane potential step, however, provides an alternative doping mechanism via exciton dissociation upon optical excitation. Indeed, dissociation is energetically favorable for a sufficiently sharp step as long as the in-plane step exceeds the binding energy of the exciton ($E_b$ ~200 meV [15]) as shown in Figure 3c. This process is similar to the well-known, junction-induced exciton dissociation process in organic photodetectors and solar cells, and is common to all semiconductors with tightly bound excitons [16]. The dissociated electron, subsequently, is able to leave via the contact resulting in a net hole photodoping process. As the photocurrent is a sensitive function of the doping in view of the above observations, for sufficient optical power, the steady-state photocurrent will be limited by the rate at which holes can be replenished – which is governed by this very edge-gate photodoping process. This becomes more evident at increasing optical power levels, when other doping mechanisms become comparatively negligible – we refer to Supplementary Figures 4–6 for further details and dual beam, power-dependent measurements confirming this picture. In addition, the doping of the sample can also be inferred from PL emission. As shown in Figure 3d, placing a strong excitation laser at the gate edge while collecting PL from the center results in onset of trion emission whenever the gate potential is greater than $E_b$ from charge neutrality (located at 0.27 V in this device). In contrast, in the absence of edge illumination, the device never accumulates holes or emits any hole-trions (Figure 3e). Interestingly, the onset of electron doping is
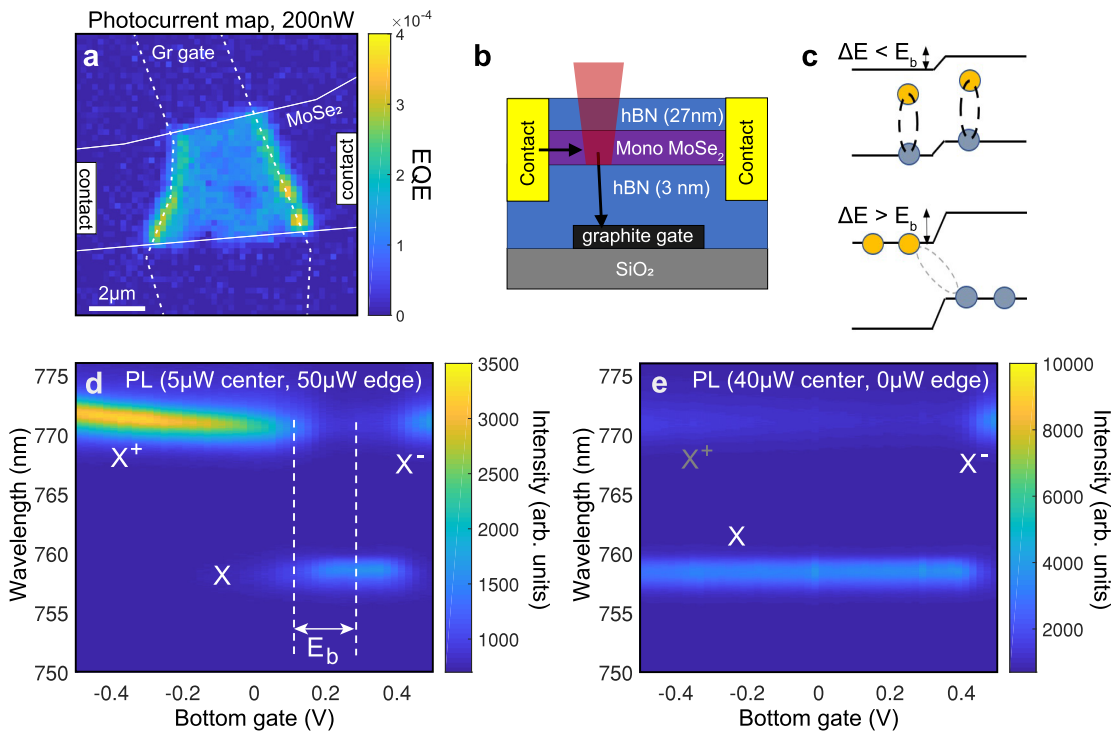


**Figure 3:** Photodoping via exciton dissociation at lateral potential steps.
a) Spatial photocurrent map of an MoSe$_2$ device (device C) with a local graphite back gate, schematic in (b), for off-resonant excitation at 660 nm. Enhanced current is seen when the excitation laser is located near an edge of the gated region, corresponding to a lateral potential step. c) Schematic of exciton dissociation at a potential step, when the step height exceeds binding energy. Due to the limited ability of Cr/Au edge contacts to inject holes into MoSe$_2$, a hole photocurrent is maintained through neutral-exciton dissociation followed by an electron current into the contacts and a hole current into the gated region. d, e) Photoluminescence (PL) spectra taken from the center of the gated region with and without 660 nm excitation at the gate edge, respectively. The onset of hole doping once the potential step exceeds $E_b$ and lack of trion oscillator strength without edge excitation indicates that photodoping is the primary mechanism for hole-doping the MoSe$_2$ structure.
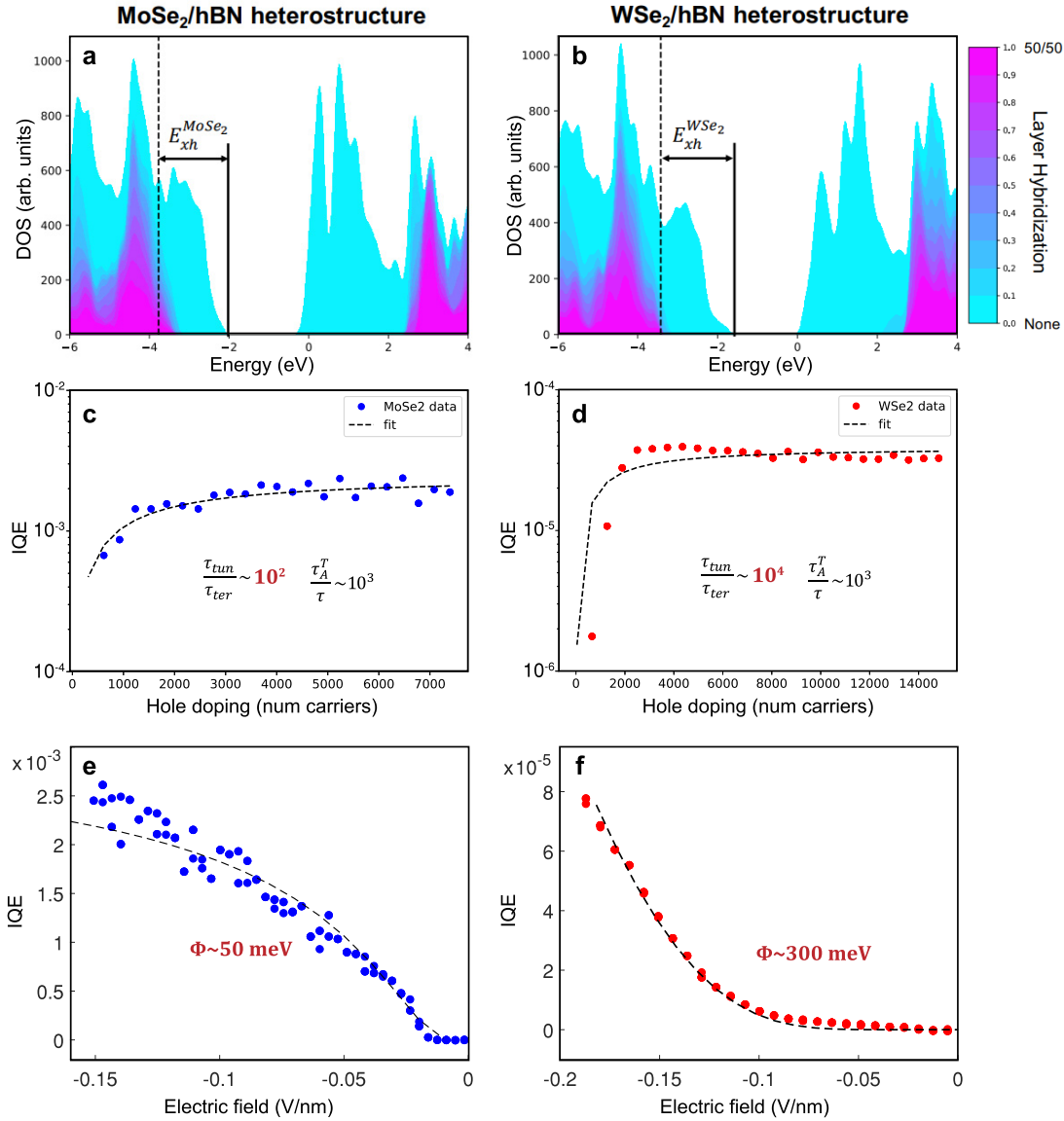
**Figure 4:** Band structure calculations and kinetics.
Density functional theory (DFT) calculations of hybridization between transition metal dichalcogenide (TMD) and hexagonal boron nitride (hBN) states for MoSe$_2$ (a), and WSe$_2$ (b) indicate a valence band offset between TMD states and layer-hybridized states on the order of the exciton energy, $E_{xh}$. c, d) Dual-gate doping dependence of photocurrent from device B fitted to extract hot hole generation rate and relative rates of tunneling and thermalization using a kinetic model. While both materials show a comparable hot hole generation, the lower internal quantum efficiency (IQE) in WSe$_2$ is explained by substantially slower tunneling relative to thermalization. IQE is obtained from the EQE data in Figure 2, after compensating for absorptivity of the TMD and photon losses in the top gate. Fitting the field-dependence of photocurrent to a Fowler–Nordheim tunneling process gives effective barriers, $\Phi$, of 50 meV in MoSe$_2$ (e) and 300 meV in WSe$_2$ (f).

unaffected as efficient charge injection can still occur via the contacts, independently of any photodoping effects.

While the former clearly illustrates the role of doping in the process, it does not yet elucidate by which mechanism holes are able to escape the TMD and penetrate or bypass the hBN barrier. For an interface between bulk crystals, a calculation of the band offset along with information about the momentum in the direction perpendicular to the interface would

provide the necessary electronic information to understand the transport across the junction. However, for an interface between a monolayer and a bulk crystal, the notion of perpendicular momentum in the monolayer is meaningless in view of the absence of periodicity in this direction. Instead, the relevant picture is one where the entire system is considered as one interface between the monolayer and the bulk. By calculating the properties of this interface, we can then obtain the relevant transport

behavior. While the exact values depend on details of the layer interface such as the orientation of the layers, interfacial reconstruction and the exact hBN layer thickness, the trends are clear and explain the observed behavior well – especially, the notable difference between $MoSe_2$ and $WSe_2$.

# 3 Physics of photocurrents

To capture the interface physics and explain the observed photocurrents, we start by using first principles methods to compute the density of states (DOS) of a bilayer system that consists of one monolayer of TMD and one monolayer of hBN, after which we color each state according to its layer hybridization (Figure 4a, b). The cyan states are unhybridized, i.e., the state is localized either entirely in the hBN layer or entirely in the TMD layer. The pure cyan states near the band gap in Figure 4a, b should thus be understood as TMD states, as the TMD band gap is much smaller than the hBN band gap. Since the layers form an interface and interact, we now also need to consider hybridization between them, which leads to delocalization across the interface. For example, the magenta states have equal weight in the TMD and hBN layer. The colors in between pure cyan and magenta indicate a state with some weight in each layer, with ratios given according to the scale bar.

To relate these DOS plots to the transmission of charge carriers from the TMD to hBN, we note that hybridized states (denoted by any color other than pure cyan) are effectively delocalized across the interface and therefore represent a pathway for a charge carrier to move between the TMD and the hBN layers. Somewhat similar to the band offset picture in bulk heterojunctions, the distance in energy from the TMD band edge (the cyan states near the gap) to the first hybridized (non-cyan) states can now be considered the effective band offset. In agreement with other studies of $MoSe_2$/hBN systems, the valence band offset is much smaller than the conduction band offset, indicating that holes can much more readily travel from the TMD to the hBN than electrons [9, 10].

These DOS plots elucidate qualitatively why the photocurrent in the $MoSe_2$ system is larger than the photocurrent in the $WSe_2$ system. They also indicate effective band offsets on the order of the excitonic energy (~1.6–1.7 eV [17, 18], see Figure 4a, b). Since our experiments take place at cryogenic temperatures (6 K), such energies are orders of magnitude higher than the thermal energy in our system. The only process capable of providing such energies is Auger recombination, where the energy of an exciton is transferred nonradiatively to a resident carrier – in our case, a hole. In the

presence of free holes, the exciton can undergo Auger recombination, during which the exciton annihilation energy is completely transferred to the hole. The hole can then scatter with a phonon in a very fast broadening process, which allows it to access hybridized states away from the K point. Consistent with the data in Figure 2c, the probability of the Auger process at low excitation intensity is linear in optical power because it requires just one exciton, in contrast to the commonly studied exciton-exciton Auger recombination, which has a quadratic dependence on excitation intensity. Due to the larger conduction band offsets between the TMD and hBN, hot electrons are unable to transfer into the hBN before thermalizing – in line with the observed electron–hole asymmetry in our experiments. In addition, Auger recombination shifts a hole to an energy with a high density of hybridized states in $MoSe_2$, while the same process in $WSe_2$ leaves the hole at an energy with a much lower density of hybridized states, as indicated by the dashed lines in Figure 4a, b. Thus, Auger recombination is much more likely to result in a hole transmitted to the hBN in the $MoSe_2$ system than in the $WSe_2$ system. This trend should persist regardless of the exact details of the junction such as the exact hBN thickness. For instance, for the sake of computational efficiency, we model a monolayer of hBN instead of the many different film thicknesses of hBN used in the experiments (see DFT methods for details). Including many layers of hBN should systematically lower the valence band maximum of the hBN in each system [19], which may introduce an additional tunneling barrier the hole must overcome. Yet, a hole in the $MoSe_2$ system would still encounter a smaller tunnel barrier than a hole in the $WSe_2$ system.

We examine the underlying Auger mechanism in greater detail by deriving the dependence of photocurrent quantum efficiency on doping from a simple kinetic model. In this model, Auger excited holes can either tunnel through an effective barrier (the aforementioned barrier minus the hot hole energy), or thermalize. By properly accounting for charge replenishment and competing (non-Auger) exciton decay paths, we can obtain approximate values for the rates of Auger recombination, hot hole thermalization and tunneling under detailed balance conditions – we refer to the Supplementary materials for details. We can use this model in combination with the deconvolved field- and doping dependence in our devices to extract relevant values. For example, fitting our model to the doping-dependence at fixed field allows us to extract approximate values for the relative times of hot-hole tunneling to thermalization ($\tau_{tun}/\tau_{ter}$) and Auger recombination relative to all exciton decay paths ($\tau_A^T/\tau$) for each system (Figure 4c, d; Supplementary material for details). We find a comparable $\tau_A^T/\tau$ of $10^3$ for both systems.
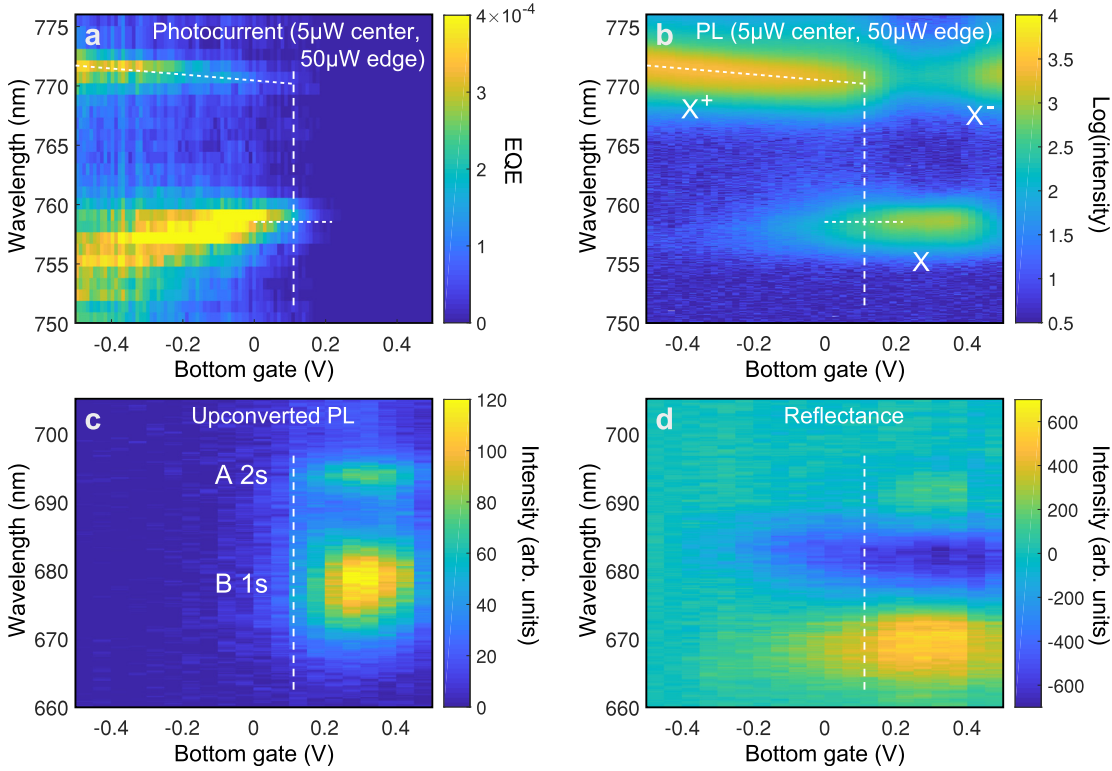
**Figure 5:** Photocurrent under resonant excitation and competition with exciton upconversion.
a) $MoSe_2$ (device C) photocurrent differential for 50 μW off-resonant gate-edge excitation and 5 μW variable-wavelength center excitation shows current following the exciton and trion resonances seen in photoluminescence (PL) in (b). c) Upconverted photoluminescence spectra taken at 759 nm excitation, documented in literature to arise from Auger excitation of the 1s A exciton, yielding emission of higher Rydberg states, along with the B exciton. d) Reflectance spectra indicating that the B exciton state persists in the hole-doped regime. The onset of hole-doping, however, corresponds to a loss of photoluminescence from the B exciton state and a corresponding onset of photocurrent, suggesting a competition between exciton–exciton Auger and exciton–hole Auger, with the latter dominating in the doped regime.

However, the relative thermalization rate (compared to tunneling) in $WSe_2$ ($10^4$) significantly exceeds that of $MoSe_2$ ($10^2$). This again reflects the higher effective tunnel barrier for $WSe_2$ as suggested by DFT. For the tunneling process itself, we consider the field dependence of the photocurrent and model it as a Fowler–Nordheim tunneling process (Figure 4e, f). The model reproduces the observed data very well, and allows us to extract effective (net) barrier heights for hot hole tunneling of 50 meV for $MoSe_2$ and 300 meV for $WSe_2$, consistent with the relative difference seen in DFT calculations.

We next consider the wavelength dependence of the photocurrent under resonant excitation, which clearly confirms the essential role of excitons, consistent with our Auger picture. Figure 5a shows the variation in gate current from the $MoSe_2$ device in Figure 3. We ensure reliable hole doping by photodoping through a strong (50 μW) above-band laser. This value exceeds that of the other rates in our system, and ensures barrier limiting (as opposed to charge-replenishment limited) behavior. When subsequently sweeping a variable wavelength laser (5 μW), we observe a

pronounced set of resonances. Comparing those against the photoluminescence emission spectrum (Figure 5b) we observe photocurrent emission coinciding with the exciton and hole-trion resonances – as expected from the perspective of an Auger picture involving excitons and holes. The substantial photocurrent from the neutral exciton in the hole-doped regime, despite low population in PL, suggests an interesting interplay between the hole-exciton scattering mechanisms that create hole-trions (also referred to as attractive polarons [20]) and Auger processes. These observations imply that photocurrent may provide an interesting probe of exciton dynamics, and could be used to shed light on varying decay mechanisms in TMDs as well as novel thermalization physics – as already suggested by our kinetic model.

Finally, we consider similarities between the photocurrent mechanism and a previously documented Auger exciton upconversion process [11]. When a TMD was excited on resonance with the lowest energy 1s exciton, PL emission was observed at higher energy (Rydberg) states [15], including the 2s exciton and B exciton from a higher

conduction band. In [11], this phenomenon was attributed to exciton–exciton annihilation, a related Auger process in which one exciton non-radiatively transfers its energy to another, hot exciton. We indeed observe this phenomenon in our MoSe$_2$ devices (Figure 5c), allowing us to examine the relationship between these processes. In reflectance measurements (Figure 5d), we observe that the B exciton state exists in both the neutral and the hole-doped regime. However, in PL, which measures population, we observe a rapid suppression of the B exciton upconverted emission with hole doping (Figure 5c), while observing the presence of a pronounced photocurrent in this regime. These observations suggest a competition between the hole-Auger process and the upconversion process: the exciton–exciton Auger process necessary to create the hot excitons that ultimately relax into the B state appears to compete with the hole-exciton Auger process. From a microscopic perspective, these observations are consistent with the relative densities of holes and excitons in our system. To first order, from a gate capacitance model, we expect a hole density of $\sim 7 \times 10^{12} \text{cm}^{-2}\text{V}^{-1}$ which exceeds the approximate exciton density of $\sim 10^{10}$ cm$^{-2}$ at only a few megavolt past the onset of hole doping. Assuming somewhat similar exciton–hole and exciton–exciton Auger recombination rates would then indeed suggest a significant suppression of upconversion upon doping due to simple competition between the two processes. More detailed analyses, with independently calibrated carrier and exciton densities, could therefore be used in combination with photocurrent and upconversion measurements to bound the ratio between these respective rates more tightly.

# 4 Outlook

In conclusion, we have shown that photoexcitation of excitons in hBN-encapsulated TMDs can give rise to a form of "photoelectric effect" for holes that results in a net and substantial current across the nominal hBN dielectric barrier. We attribute this effect due to Auger-generated hot holes being swept through the barrier by the electric field in a tunneling process, which we substantiate by careful field, doping, wavelength and power dependencies. We further support our claims with detailed, ab initio calculations that match well with our observations of a systematically higher effective hole tunnel barrier for WSe$_2$ as compared to MoSe$_2$. In addition to shedding light on the intrinsic Auger effects in TMDs, which are important to evaluate their device performance as photodetectors and other optoelectronic devices, our studies also demonstrate the spectroscopic potential of photocurrent studies, and

provide a novel probe to study non-radiative effects such as carrier thermalization in 2D semiconductors. Intriguingly, if further studies confirm a certain degree of coherence in the photoelectric effect, our findings may open the door for on-chip, integrated probing of the local density of states – in a way similar to advanced spectroscopic techniques such as ARPES, but with greatly reduced complexity and with nanoscale resolution.

# References

[1] S. Manzeli, D. Ovchinnikov, D. Pasquier, O. V. Yaziev, and A. Kis, "2D transition metal dichalcogenides," *Nat. Rev. Mater.*, vol. 2, p. 17033, 2017.

[2] K. F. Mak and J. Shan, "Photonics and optoelectronics of 2D semiconductor transition metal dichalcogenides," *Nat. Photonics*, vol. 10, p. 216, 2016.

[3] A. K. Geim and I. V. Grigorieva, "Van der Waals heterostructures," *Nature*, vol. 499, p. 419, 2013.

[4] R. Bekenstein, I. Pikovski, H. Pichler, E. Shahmoon, S. F. Yelin, and M. D. Lukin, "Quantum metasurfaces with atom arrays," *Nat. Phys.*, vol. 16, p. 676, 2020.

[5] G. Scuri, Y. Zhou, A. High, et al., "Large excitonic reflectivity of monolayer MoSe$_2$ encapsulated in hexagonal boron nitride," *Phys. Rev. Lett.*, vol. 120, p. 037402, 2018.

[6] C. R. Dean, A. F. Young, I. Meric, et al., "Boron nitride substrates for high-quality graphene electronics," *Nat. Nanotechnol.*, vol. 5, p. 722, 2010.

[7] M. Yankowitz, Q. Ma, P. Jarillo-Herrero, and B. J. LeRoy, "van der Waals heterostructures combining graphene and hexagonal boron nitride," *Nat. Rev. Phys.*, vol. 1, p. 112, 2019.

[8] G. Cassabois, P. Valvin, and B. Gil, "Hexagonal boron nitride is an indirect bandgap semiconductor," *Nat. Photonics*, vol. 10, p. 262, 2016.

[9] E. Linardy, D. Yadav, D. Vella, et al., "Harnessing exciton–exciton annihilation in two-dimensional semiconductors," *Nano Lett.*, vol. 20, p. 1647, 2020.

[10] C. M. E. Chow, H. Yu, J. R. Schaibley, et al., "Monolayer semiconductor Auger detector," *Nano Lett.*, vol. 20, no. 7, pp. 5538–5543, 2020.

[11] B. Han, C. Robert, E. Courtade, et al., "Exciton states in monolayer MoSe2 and MoTe2 probed by upconversion spectroscopy," *Phys. Rev. X*, vol. 8, p. 031073, 2018.

[12] N. M. Gabor, J. C. W. Song, Q. Ma, et al., "Hot carrier–assisted intrinsic photoresponse in graphene," *Science*, vol. 334, p. 648, 2011.

[13] Q. Ma, T. I. Andersen, N. Nair, et al., "Tuning ultrafast electron thermalization pathways in a van der Waals heterostructure," *Nat. Phys.*, vol. 12, p. 455, 2016.

[14] K. J. Tielrooij, J. C. W. Song, S. A. Jensen, et al., "Photoexcitation cascade and multiple hot-carrier generation in graphene," *Nat. Phys.*, vol. 9, p. 248, 2013.

[15] A. Chernikov, T. C. Berkelbach, H. M. Hill, et al., *Phys. Rev. Lett.*, vol. 113, p. 076802, 2014.

[16] M. Massicotte, F. Vialla, P. Schmidt, et al., "Dissociation of two-dimensional excitons in monolayer WSe$_2$," *Nat. Commun.*, vol. 9, p. 1633, 2018.

[17] S. Shree, M. Semina, C. Robert, et al., "Observation of exciton-phonon coupling in MoSe2 monolayers," *Phys. Rev. B*, vol. 98, p. 035302, 2018.

[18] E. Courtade, M. Semina, M. Manca, et al., "Charged excitons in monolayer WSe2: Experiment and theory," *Phys. Rev. B*, vol. 96, p. 085302, 2017.

[19] D. Wickramaratne, L. Weston, and C. G. Van de Walle, "Monolayer to bulk properties of hexagonal boron nitride," *J. Phys. Chem. C*, vol. 122, p. 25524, 2018.

[20] M. Sidler, P. Back, O. Cotlet, et al., "Fermi polaron-polaritons in charge-tunable atomically thin semiconductors," *Nat. Phys.*, vol. 13, p. 255, 2016.